GLIA

WILEY

RESEARCH ARTICLE

Carbon monoxide controls microglial erythrophagocytosis by regulating CD36 surface expression to reduce the severity of hemorrhagic injury

Sandra Kaiser[1,2] | Lisa Selzner[1,2] | Janick Weber[1,2] | Nils Schallner[1,2]

[1]Department of Anesthesiology & Critical Care Medicine, Medical Center, University of Freiburg, Germany

[2]Faculty of Medicine, University of Freiburg, Germany

Correspondence
Dr. Nils Schallner, Department of Anesthesiology & Critical Care Medicine, Medical Center—Faculty of Medicine, University of Freiburg, Hugstetter Str. 55, 79106 Freiburg, Germany.
Email: nils.schallner@uniklinik-freiburg.de

Abstract

Microglial erythrophagocytosis is crucial in injury response to hemorrhagic stroke. We hypothesized that regulation of microglial erythrophagocytosis via HO-1/CO depends on a pathway involving reactive oxygen species (ROS) and CD36 surface-expression. The microglial BV-2 cell line and primary microglia (PMG) were incubated +/−blood and +/−CO-exposure. PMG isolated from tissue-specific HO-1-deficient (*LyzM-Cre-Hmox1*$^{fl/fl}$) and *CD36*$^{-/-}$ mice or siRNA against *AMPK* (AMP-activated protein kinase) were used to test our hypothesis. In a murine subarachnoid hemorrhage (SAH) model, we compared neuronal injury in wild-type and *CD36*$^{-/-}$ mice. Readouts included vasospasm, microglia activation, neuronal apoptosis, and spatial memory. We observed increased microglial HO-1-expression after blood-exposure. A burst in ROS-production was seen after CO-exposure, which led to increased amounts of phosphorylated AMPK with subsequently enhanced CD36 surface-expression. Naïve PMG from *LyzM-Cre-Hmox1*$^{fl/fl}$ mice showed reduced ROS-production and CD36 surface-expression and failed to respond to CO with increased CD36 surface-expression. Lack of HO-1 and CD36 resulted in reduced erythrophagocytosis that could not be rescued with CO. Erythrophagocytosis was enhanced in BV-2 cells in the presence of exogenous CO, which was abolished in cells treated with siRNA to AMPK. *CD36*$^{-/-}$ mice subjected to SAH showed enhanced neuronal cell death, which resulted in impaired spatial memory function. We demonstrate that microglial phagocytic function partly depends on a pathway involving HO-1 with changes in ROS-production, phosphorylated AMPK, and surface expression of CD36. CD36 was identified as a crucial component in blood clearance after hemorrhage that ultimately determines neuronal outcome. These results demand further investigations studying the potential neuroprotective properties of CO.

KEYWORDS

brain hemorrhage, carbon monoxide, heme oxygenase, microglia, phagocytosis

---

Sandra Kaiser and Lisa Selzner contributed equally to this study.

1 | INTRODUCTION

The pathophysiology of neuronal injury after aneurysmal subarachnoid hemorrhage (SAH), a hemorrhagic stroke subtype with high mortality and early average age of onset, remains poorly understood (King Jr., 1997; Rincon, Rossenwasser, & Dumont, 2013; van Lieshout et al., 2017). Many patients suffer long-term cognitive impairment attributable to early brain injury (EBI) (Suwatcharangkoon et al., 2016) or delayed cerebral ischemia (DCI) (Hijdra et al., 1986). The longstanding dogma of cerebral vasospasm being the decisive component that determines neuronal injury has been challenged by recent clinical data aiming to effectively treat vasospasm (Macdonald et al., 2011). We have previously demonstrated that the deposition of heme-containing blood components is a critical factor in the determination of neuronal injury and that clearance of blood can help to reduce brain injury and neurocognitive deficits (Schallner et al., 2015). The cells identified to play a crucial role in hemorrhage resolution are microglia, the immunocompetent cells of the brain. Elimination of heme occurs via the heme oxygenase (HO) enzyme system degrading heme to biliverdin, iron, and carbon monoxide (CO). The HO-1 isoform is ubiquitously expressed and can be strongly induced. The HO-2 isoform is constitutively expressed in selected tissues including the brain, endothelium, and testes. HO-1 has strong cytoprotective properties demonstrated in various disease models including visceral organ injury (Otterbein, Kolls, et al., 1999; Tayem, Green, Motterlini, & Foresti, 2014; Zuckerbraun et al., 2003), cardiac ischemia–reperfusion (Clark et al., 2000) and the central nervous system (Chen, Fang, Zhang, Zhou, & Wang, 2011; Foresti et al., 2013; Shimada et al., 2009; Wang, Xu, & Zhu, 2012; Zhang et al., 2012). Cerebral HO expression patterns show a distinct spatial and cell-specific distribution: HO-2 is constitutively expressed in neuronal cells and expression is not changed during ischemic or hemorrhagic injury (P. Matz et al., 1996; Sutherland et al., 2009). In contrast, HO-1 is barely expressed in healthy nervous tissue, but strongly upregulated in glial cells after injury (Fukuda, Panter, Sharp, & Noble, 1995; Kuroki, Kanamaru, Suzuki, Waga, & Semba, 1998; P. Matz et al., 1996; P. G. Matz, Weinstein, & Sharp, 1997; Sutherland et al., 2009; Turner, Panter, & Sharp, 1999). Only a few reports have examined the protective effects of exogenously given CO gas on neuronal cells (Almeida, Queiroga, Sousa, Alves, & Vieira, 2012; Schallner et al., 2012; Vieira, Queiroga, & Alves, 2008; Zeynalov & Dore, 2009). In fact, the majority of reports over the last decades picture CO as a potent neurotoxic agent. However, exogenous application of CO gas can be cytoprotective similar to HO-1 induction (Goebel et al., 2008; Motterlini & Otterbein, 2010; Otterbein, Mantell, & Choi, 1999; Song et al., 2003; Yabluchanskiy et al., 2012) and can compensate the absence of endogenous CO production via HO-1 (Schallner et al., 2015).

We have previously reported that microglial HO-1 with subsequent endogenous CO production critically determines microglial phagocytic activity (Schallner et al., 2015). The exact mechanisms of how the HO-1-CO axis modulates microglial phagocytosis of erythrocytes after brain hemorrhage remains poorly understood. The class B scavenger receptor CD36 facilitates recognition and phagocytosis of apoptotic cells (Fadok, Warner, Bratton, & Henson, 1998) and erythrocytes (McGilvray, Serghides, Kapus, Rotstein, & Kain, 2000) by cells of the innate immune system and determines hematoma resolution after hemorrhagic stroke (Fang et al., 2014; Flores et al., 2016; Mu, Wang, Hang, Liu, & Wu, 2017). The mechanisms how CD36 might be regulated via the HO-1/CO axis have not been studied.

Due to its high affinity to heme-containing groups, intracellular signaling of CO is manifold and involves various intracellular structures including the mitochondria. Mitochondrial reactive oxygen species (ROS) production after CO exposure could serve as an intracellular signal influencing downstream targets critical for phagocytic function. This includes AMP-activated protein kinase (AMPK) that has been shown to be involved in phagocytosis (Jiang et al., 2013). In this study we provide data demonstrating that the ability of the HO-1/CO signaling axis to enhance erythrophagocytosis after hemorrhage is in part due to a ROS-dependent activation of AMPK with subsequent changes in CD36 surface expression. We therefore define a novel mechanism for the regulation of CD36 as a crucial component during hemorrhage resolution and attenuation of neuronal injury following hemorrhagic injury.

2 | MATERIALS AND METHODS

2.1 | Animals and anesthesia

Wild-type (*WT*) male C57BL/6 (#000664) and CD36-deficient (*CD36*$^{-/-}$) (#019006) mice were obtained from the Jackson Laboratory. Cell-specific HO-1 knockout in microglia (*LyzMCre-Hmox1*$^{fl/fl}$) was achieved by crossing *Hmox1*$^{fl/fl}$ mice (Riken Bio Resource Center, RBRC03163) with mice expressing Cre recombinase under the lysozyme (Lyz) promoter (Jackson Laboratory, #004781). As *Hmox1*$^{fl/fl}$ and *CD36*$^{-/-}$ mice share the same C57BL/6 background, *Hmox1*$^{fl/fl}$ microglia were used as controls for all in vitro studies. Animals were fed with standard rodent diet ad libitum while kept on a 12-hr light/12-hr dark cycle. All types of surgery and manipulations were performed under general anesthesia with ketamine (100 mg/kg) and xylazine (5 mg/kg) and body temperature maintenance. At surgery, buprenorphine (50 μg/kg) was applied subcutaneously to treat possible pain.

2.2 | Subarachnoid hemorrhage (SAH) stroke model

SAH was achieved by pre-chiasmatic injection of autologous blood. In brief, after induction of anesthesia, the head was fixed in a stereotactic apparatus. With a midline incision, the skin overlying the anterior skull was opened. 3.5 mm anterior to the bregma, a burr hole was drilled into the skull with a caudal angel of 40°, using a 0.8 mm drill. 40 μl of blood was withdrawn from a C57BL/6 *WT* blood donor and injected over 30 s with a 27-G needle advanced through the burr hole at a 40° angle until the base of the skull was reached. The needle was left in place for 1 min to avoid backflow. After skin suture, animals were allowed to emerge from anesthesia under close supervision with body temperature maintenance using infrared light. The mice were

treated with buprenorphine (50 μg/kg) after the intervention three times a day for the first 3 days postoperative.

2.3 | CO gas treatment

After SAH, *WT* and *CD36*$^{-/-}$ animals were randomly assigned to either receive treatment with CO or synthetic air for 1 hr. CO exposure was done in a custom-made gas exposure chamber. Animals had free access to food and water during the exposure. 1% CO gas was mixed with synthetic air to achieve 250 ppm. CO concentration was monitored continuously throughout the application by an infrared gas analyzer. Treatment was started immediately after the SAH procedure and repeated every 24 hr for 7 days.

2.4 | Barnes maze behavioral studies

Cognitive function and spatial learning were tested on the Barnes maze as described previously, with minor modification. In brief, the paradigm consisted of a white circular platform with a diameter of 120 cm. Along the perimeter of the platform, 40 equal-sized holes were located. One hole led to a box to which the animals could escape from the open platform. As an aversive stimulus, a bright light source was placed above the platform. We introduced an additional reward stimulus by placing food in the escape box. Cardboard placards with different visual cues were placed around the platform. The location of the escape box and the visual cues were kept constant during the initial acquisition period. Prior to SAH, the mice underwent spatial acquisition for 7 days, with three trials per animal per day. Animals were allowed to explore the maze for 3 min. Once they entered the escape box, they were allowed to remain in the box for 30 s. The inter-trial interval was 30 min for each animal, with extensive cleaning of the platform after each animal to eliminate olfactory cues. Animals that did not enter the escape box within 3 min were guided to the correct hole. Surrogates for cognitive function were measured: specifically, the total time required for the mouse to find the goal box (latency) and the number of holes the animal explored before finding the goal box (error number). After 7 days of acquisition, SAH was performed as described above. Spatial memory testing, which consisted of one trial per animal per day, was started on day 1 after SAH and continued for 7 days. To test for flexibility and relearning, the location of the goal box was moved 180° from its original position on day 4 (spatial reversal), while visual cues were kept at the initial position. Maze procedures were performed by an investigator blinded to the genotype and treatment groups.

2.5 | Hematoxylin/eosin staining and evaluation of cerebral vasospasm

Seven days after SAH, animals were deeply anesthetized with ketamine and xylazine and transcardially perfused with TBS followed by PFA 4%. Brains were removed and postfixed in PFA 4% for 18 hr.

After cryoprotection in sucrose, brains were frozen, cut in 9 μm sections and stained with hematoxylin and eosin. Representative digital images of three consecutive middle-cerebral artery (MCA) cross-sections from each animal were obtained and the lumen radius/wall thickness ratio was quantified to assess vasospasm using Image J.

2.6 | Immunohistochemistry

Frozen brains were cut in 9 μm serial coronal sections. The glass slides with brain sections were heated in 1x citrate buffer pH 6 (Zytomed System GmbH, K035) in a microwave (3x5 min 800 W). Permeabilization was done with 0.1% Triton/PBS for 10 min at room temperature (Iba-1) or ice-cold Methanol for 10 min at −20°C (cleaved Caspase-3) or with 0.2% Tween/PBS for 10 min at room temperature (TER-119 co-staining with Iba-1). Slides were then blocked in 10% donkey serum/PBS (Iba-1 or Caspase-3 or 4% BSA/PBS (TER-119 co-staining with Iba-1) for 1 hr at room temperature. Staining was performed with primary antibodies against Iba-1 (Abcam AB5076, 1:200), cleaved Caspase-3 (Cell Signaling 9664S, 1:100) or against TER-119 (Abcam AB91113, 1:100) at 4°C overnight. Sections were then conjugated with the corresponding secondary antibody for fluorescent imaging (for Iba-1 anti-goat Alexa Fluor 488, Abcam AB150129, for cleaved Caspase-3 anti-rabbit Alexa Fluor 488, Abcam AB150073and for TER-119 anti-rat Alexa Fluor 555, Abcam AB150154; 1:300). Nuclear counterstain was done with Hoechst 33258 (Sigma, 1:10,000, 5 min) and slides were examined under a fluorescence microscope (Zeiss AxioObserver Invert). To achieve appropriate consistency in quantification of cells, from each area of interest 4 images were obtained of 3 mice per group. For apoptotic cell quantification, cleaved Caspase-3 and DAPI positive cells were counted. For analysis of microglia phagocyting erythrocytes, cells with colocalization of TER-119 and Iba-1 where counted. The morphology of activated microglia is characterized by larger cells with retracted extensions while resting microglia are smaller with larger ramifications. Thus, we measured the soma size of Iba-1 positive microglia by area with ZEN 2.5 (blue edition) software from Carl Zeiss Microscopy.

2.7 | BV-2 and PMG cell culture and treatment

BV-2 microglia cells were incubated in DMEM containing 1% penicillin–streptomycin and 10% FBS in a humidified atmosphere with 5% CO_2. Cells were seeded into 6-well plates at a density of 200,000 for individual experiments. PMG from *WT*, *CD36*$^{-/-}$, *Hmox1*$^{fl/fl}$, or *LyzMCre-Hmox1*$^{fl/fl}$ were isolated from mice at P5 to P7 by enzymatic neural dissociation (Papain Neural Dissociation Kit; Miltenyi Biotec) and in vitro mixed glia culture. In brief, mouse brains were enzymatically dissociated according to the manufacturer's instructions, and the resulting mixed glia culture containing astrocytes and microglia was cultivated in DMEM containing 1% penicillin–streptomycin, 10% FBS, and M-CSF (10 ng/ml) in a humidified atmosphere with 5% CO_2. After

1 week of cultivation, cell culture plates were shaken at 200 rpm for 30 min every 2 to 3 days. Floating microglia were collected from the supernatant and seeded onto 6-well plates for experiments at a density of 2×10^5 cells per well. Microglial phenotype was confirmed by CD11b staining and flow cytometry.

For erythrophagocytosis experiments, 100 µl blood was drawn from the mandibular vein of a C57BL/6 *WT* animal, washed with PBS, and stained with 356 µM amine-reactive, pH-sensitive fluorescent ester dye (pHrodo Green STP Ester; Thermo Fisher Scientific) in 1 ml PBS for 30 min. PMG were incubated with 100 µl labeled red blood cell suspension for various durations as indicated in the individual experiments. Cells in which we wanted to study the role of CO were transferred to an air-tight, humidified chamber (C-Chamber;

Biospherix) after starting the red blood cell exposure and exposed to 250 ppm CO, 21% O_2 and 5% CO_2 for various durations, which was controlled by an automated gas delivery system (Oxycycler; Biospherix). For pharmacological inhibition of HO-1, 100 µM SnPP IX was used (Cayman Chemical, 15 min preincubation). For scavenging of ROS, we used 500 µM of N-Acetylcysteine (NAC, Sigma, overnight preincubation).

2.8 | Flow cytometry

PMG were harvested with a cell lifter, washed with flow cytometric buffer (PBS with 1% BSA, 2 mM EDTA, and 0.05% Na-azide), blocked
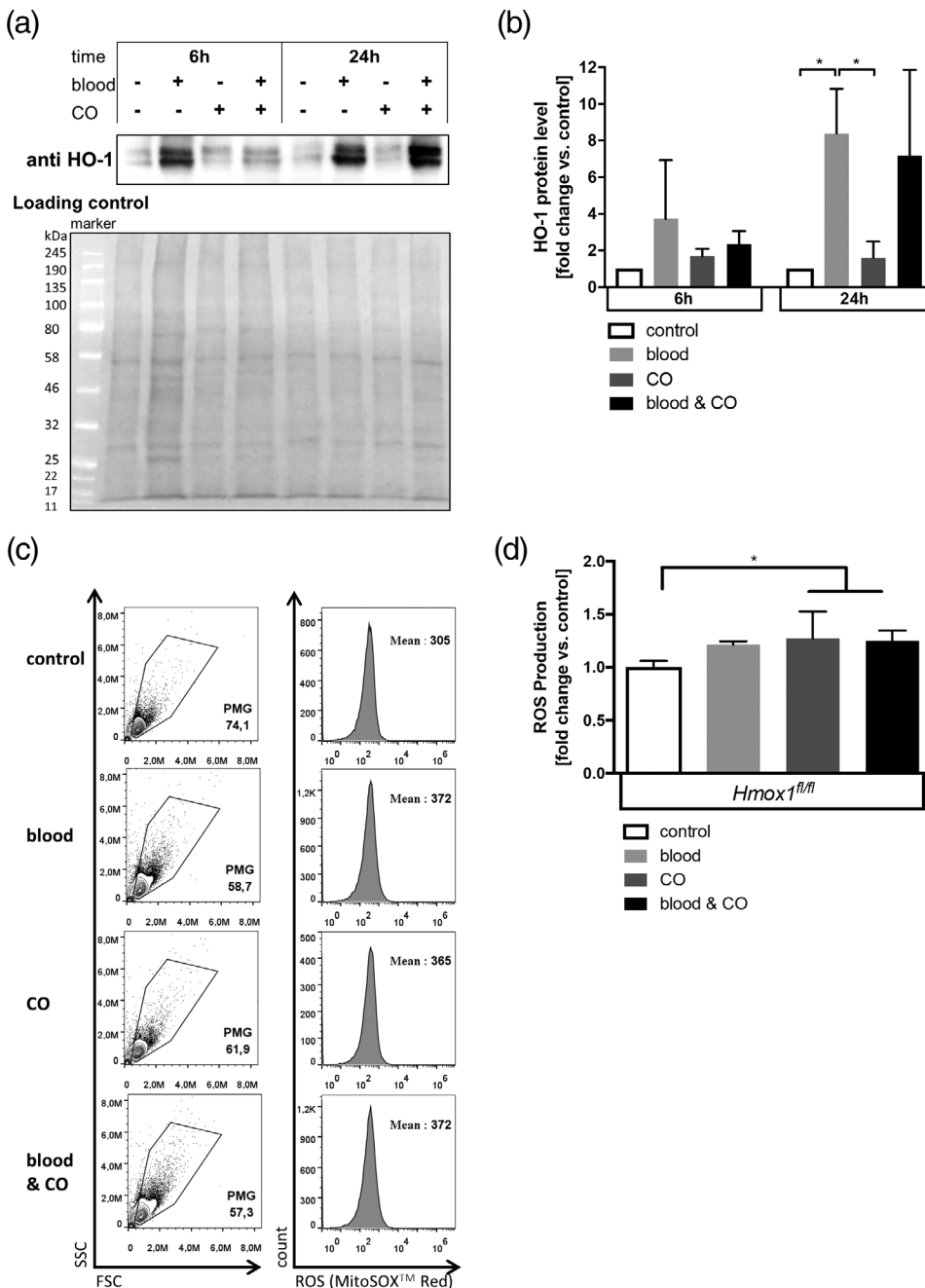
FIGURE 1 Induction of HO-1 after exposure of microglia to blood. (a) Representative Western blotting showing time-dependent HO-1 protein levels in response to exposure to blood (10 µl, 6 or 24 hr) and CO (250 ppm, 1 hr) in BV-2 microglia. Double bands are due to antibody reactivity against the truncated form of HO-1. Lower panel shows corresponding loading control using total protein staining. (b) Statistical analysis of Western blot densitometry of n = 3 blots per condition. Analysis of HO-1 protein levels normalized to total protein loading control. Shown as fold change versus 6 hr control and 24 hr control, respectively. *p* = .02 control versus blood 24 hr, *p* = .05 blood versus CO 24 hr. (c and d) Mitochondrial ROS-production measured using MitoSox dye (c, representative flow cytometry dot plots and histograms) and quantified as fold change versus control (d) in microglia isolated from *Hmox-1^fl/fl^* mice with normal HO-1 expression. Cells were harvested 5 min after beginning of gas/blood exposure. n = 6 experiments per condition. *p* = .02 control versus CO, *p* = .03 control versus blood & CO. ROS, reactive oxygen species

with CD16/32 antibody (Biolegend 101320, 15 min on ice) and stained with antibodies against CD36 and CD11b (both Biolegend 102608 and 101216, 1:100, 30 min on ice). Flow cytometry was performed on a flow cytometer (Attune, Applied Biosystems), with selection of CD11b-positive PMG and detection of phagocytosis-related fluorescence and changes in CD36 surface expression, respectively. The relative percentage of positive PMG and the mean fluorescence per PMG were calculated using FlowJo software.

2.9 | Western blot analysis

Cells were washed with PBS and lysed in radioimmunoprecipitation assay (RIPA) buffer with PhosStop (Sigma Aldrich 4906845001) and proteaseinhibitor (Sigma Aldrich 4693116001) shaking with

1,000 rpm for 10 min at 4°C. Equal amounts of protein were separated on a 10% SDS (Sigma-Aldrich R0278) polyacrylamide gel (TGX Stain-Free™ FastCast™ 161–0183 Bio-Rad) and transferred to a polyvinylidene difluoride (PVDF) membrane (Trans Blot Turbo Transfer Pack 1704157 Bio-Rad) with a Trans Blot Turbo Transfer System (Bio-Rad). Pictures of the membrane were recorded under UV light for total protein display. Membranes were blocked with 5% skim milk BSA in Tween-20/TBS and incubated in the recommended dilution of specific antibodies (Abcam: HO-1 AB52947, AMPKα1 32047; Cell Signaling: AMPKα 5,832, p-AMPK 2535, 1:1,000) overnight at 4°C. Membranes were then incubated with the corresponding secondary antibody 1:5000 for chemiluminescence detection and developed on a Fusion FX imaging system with Western Lightning Plus-ECL (Perkin Elmer NEL103001EA). For normalization, total protein staining was used.
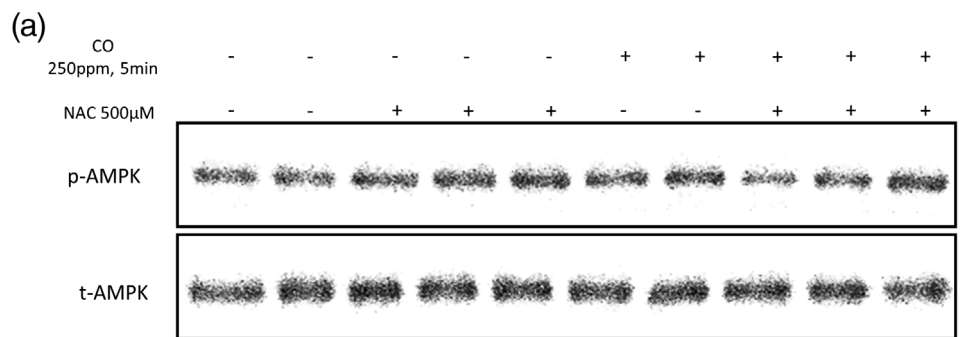
FIGURE 2 Phosphorylated AMPK and CD36 surface expression increases with CO exposure. (a) Representative Western blot showing time-dependent protein level of phosphorylated AMPK in response to exposure to CO (250 ppm, 5 min) and NAC (500 μM) in relation to total AMPK protein in BV-2 microglia. (b) Statistical analysis of Western blot densitometry of $n = 3$ blots per condition. Analysis of protein levels of phosphorylated AMPK +/−NAC +/−CO. $p = .04$ native versus CO; $p = .004$ CO versus NAC & CO. (c and d) CD36 surface expression measured by using flow cytometry (c, representative flow cytometry dot plots and histograms) and quantified as fold change versus control (d) in microglia isolated from $Hmox-1^{fl/fl}$ mice with normal HO-1 expression. Cells were harvested 5 min after beginning of gas/blood exposure. $n = 6$ experiments per condition. $p = .05$ control versus CO
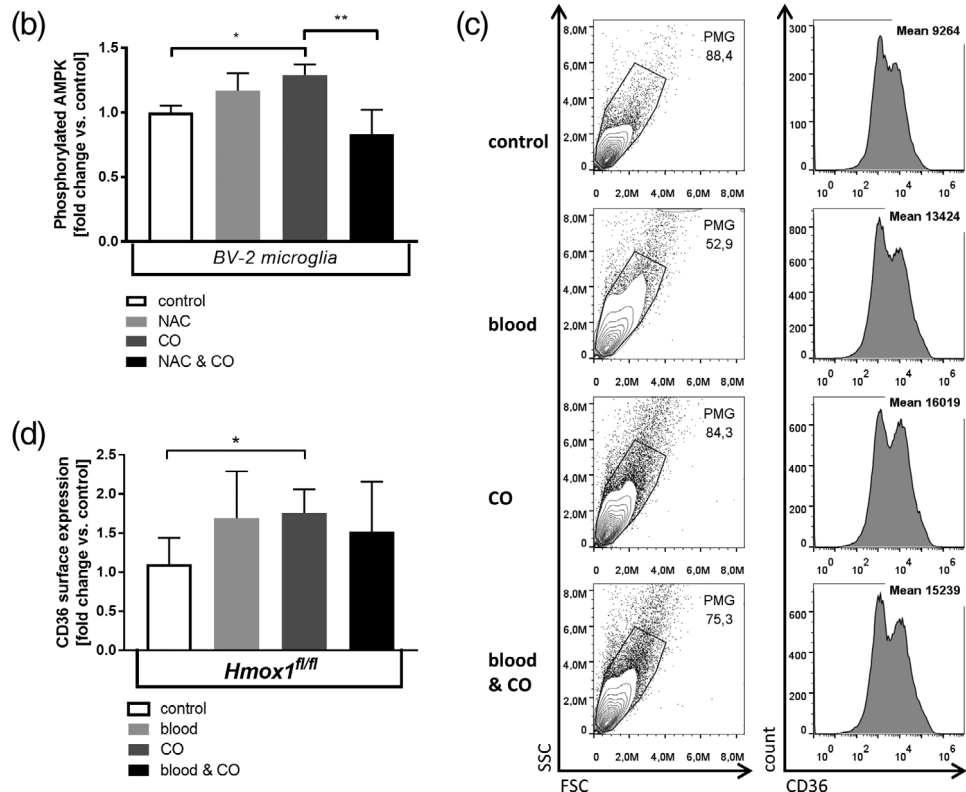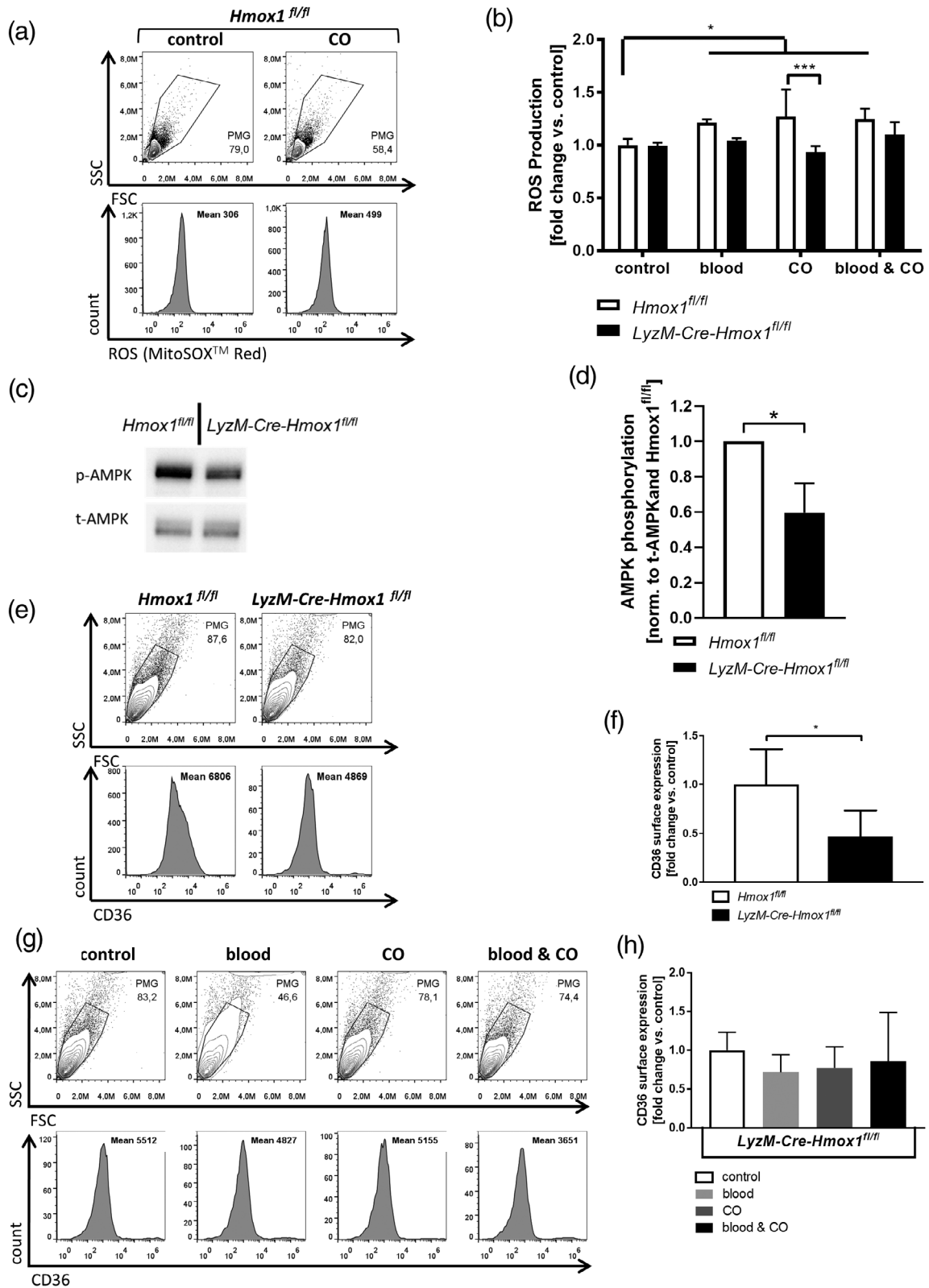
FIGURE 3   Legend on next page.

2.10 | CBA assay

PMG were incubated with blood +/−CO at the indicated concentration and time. Cell supernatant was harvested to be analyzed using bead-based flow cytometry as per manufacturer's instructions (BD 552364, Mouse Inflammation Kit). The following targets were measured on a BD Fortessa flow cytometer: IL-6, IL-10, MCP-1, IFN-γ, TNF, IL-12p70. Data were analyzed with FCAP Array™ Software.

2.11 | Quantification of ROS production

Mitochondrial ROS production was evaluated using a superoxide-sensitive dye (MitoSox red, Thermo Fisher Scientific M36008). Cells were loaded with the indicator dye prior to intervention following the manufacturer's recommendation. Mitochondrial ROS production was quantified using flow cytometry.

2.12 | RNA interference

RNA interference in BV-2 cells was done using Lipofectamine (Invitrogen) according to the manufacturer's instruction. Cells were either transfected with siRNA specifically against the catalytic subunit of AMPK (anti-AMPKα1, sense: GGAGAGCUAUUUGAUUAUAdTdT; antisense: UAUAAUCAAAUAGCUCUCCdTdT; Eurogentec) or non-sense siRNA (24 hr 50 nM). Cells were then subjected to downstream analyses as indicated.

2.13 | Statistics

Data were analyzed with a computerized statistical program (GraphPad Prism Version 7). Results are presented as means (±*SD*). Two groups were compared with Student's *t*-test, while multiple groups were compared with one-way ANOVA with post hoc Tukey multiple comparison. For grouped data with two variables (e.g., genotype and intervention), two-way ANOVA with post hoc

Tukey test was used. A *p*-value smaller than .05 was considered to be statistically significant.

2.14 | Study approval

All procedures involving the animals were approved by the Committee of Animal Care of the University of Freiburg (Permit No. G15/61) and conducted in accordance with the ARRIVE guidelines.

3 | RESULTS

3.1 | Microglia exposed to blood show elevated expression of HO-1

As HO-1 activity contributes to heme breakdown and removal, we first studied whether BV-2 microglia show induction of HO-1 expression in response to incubation with blood in vitro. Western blot analysis (Figure 1a,b) showed that HO-1 is upregulated in microglia in a time-dependent manner, indicating increased heme breakdown after erythrophagocytosis in these cells.

3.2 | Microglia produce mitochondrial ROS after exposure to CO

Due to elevated HO-1 activity during heme breakdown, increasing amounts of CO are produced endogenously. As a gasotransmitter and intracellular signaling molecule, CO binds to heme-containing structures within the cell, including the mitochondrial respiratory chain. We tested whether this leads to increased production of reactive oxygen species of mitochondrial origin, which can serve as intracellular messengers. Using flow cytometry and a specific dye that binds to mitochondrial ROS, we observed increased production of mitochondrial ROS after in vitro CO-exposure of control microglia expressing HO-1 (*Hmox1*$^{fl/fl}$) (Figure 1c,d). In addition, when microglia were exposed to blood during CO exposure, microglia cell cultures showed a similar increase in ROS production without an additive effect.

FIGURE 3 Impaired ROS-CD36 signaling in *LyzMCre-Hmox1*$^{fl/fl}$ microglia. (a and b) Mitochondrial ROS production measured using MitoSox dye (a, representative images) and quantified as fold change versus control (b) in microglia isolated from *Hmox-1*$^{fl/fl}$ and *LyzMCre-Hmox1*$^{fl/fl}$ mice. Cells were harvested 5 min after beginning of gas/blood exposure. n = 6 experiments per condition. *p* = .05 control *Hmox-1*$^{fl/fl}$ versus blood *Hmox-1*$^{fl/fl}$; *p* = .005 control *Hmox-1*$^{fl/fl}$ versus CO *Hmox-1*$^{fl/fl}$; *p* = .007 control *Hmox-1*$^{fl/fl}$ versus blood & CO *Hmox-1*$^{fl/fl}$; *p* = .0005 CO *Hmox-1*$^{fl/fl}$ versus *LyzMCre-Hmox1*$^{fl/fl}$. (c) Representative Western blot image of phosphorylated AMPK in *Hmox-1*$^{fl/fl}$ versus *LyzMCre-Hmox1*$^{fl/f}$ microglia in relation to total AMPK protein. (d) Statistical analysis of Western blot densitometry of n = 4 blots per genotype *Hmox-1*$^{fl/fl}$ and *LyzM-Cre-Hmox1*$^{fl/fl}$. Analysis of protein levels of phosphorylated AMPK normalized (norm.) to total AMPK and *Hmox-1*$^{fl/fl}$, *p* = .017. (e and f) CD36 surface expression measured by using flow cytometry (e, representative flow cytometry dot plots and histograms) and quantified as fold change versus control (f) in microglia isolated from *Hmox-1*$^{fl/fl}$ and *LyzMCre-Hmox1*$^{fl/fl}$ mice. n = 6 experiments per condition. *p* = .02 *Hmox-1*$^{fl/fl}$ versus *LyzMCre-Hmox1*$^{fl/fl}$. (g and h) CD36 surface expression measured by using flow cytometry (g, representative flow cytometry dot plots and histograms) and quantified as fold change versus control (h) in microglia isolated from *LyzMCre-Hmox1*$^{fl/fl}$ mice +/−blood and +/−CO (250 ppm). Cells were harvested 5 min after beginning of gas/blood exposure. n = 6 experiments per condition. *p* = n.s. for all comparisons. ROS, reactive oxygen species
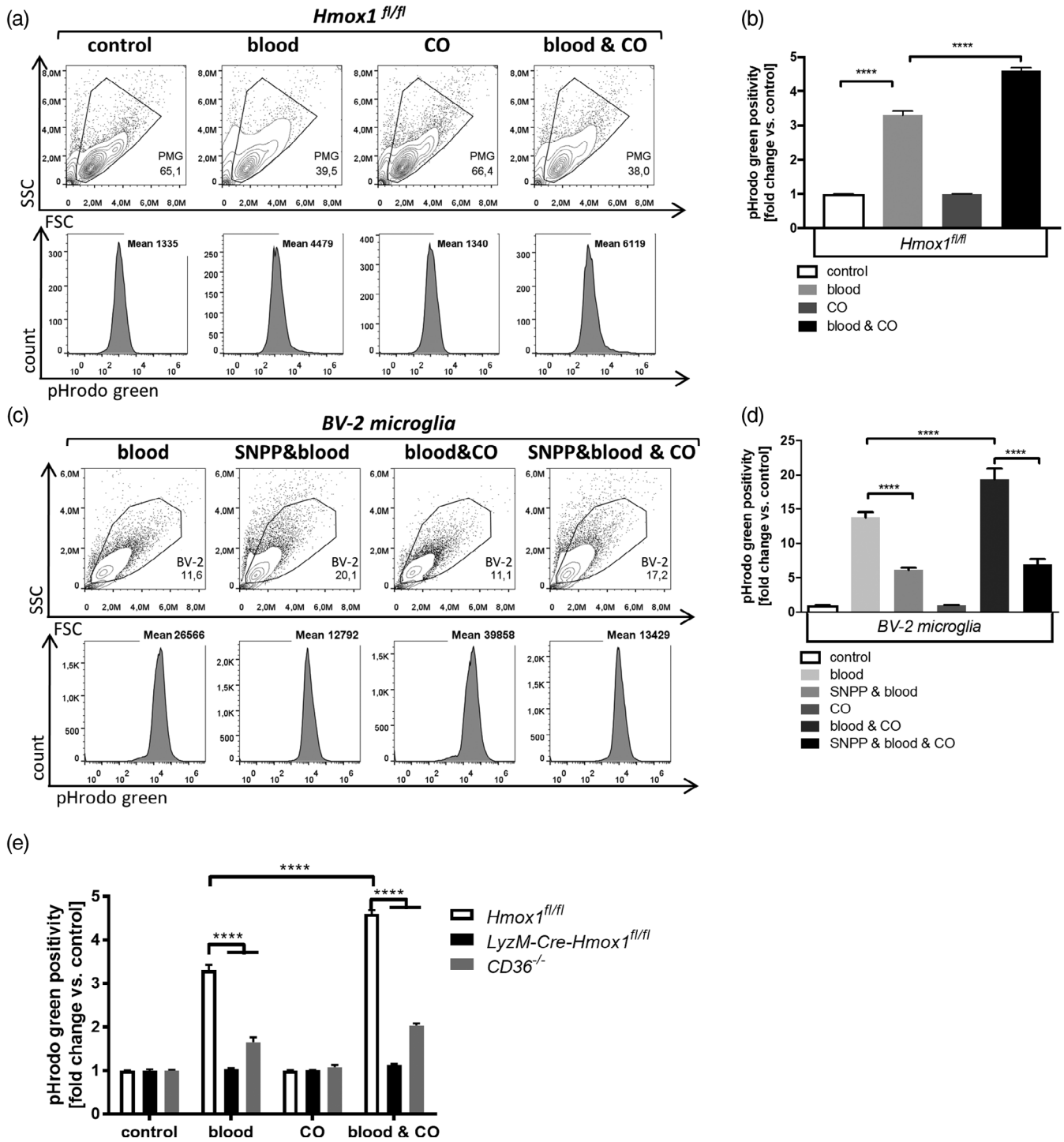
FIGURE 4 Impaired erythrophagocytosis in *LyzMCre-Hmox1^fl/fl^* and *CD36^−/−^* microglia. (a and b) Effect of CO on erythrophagocytosis in *Hmox-1^fl/fl^* microglia analyzed by flow cytometry after fluorescent blood labeling with phrodo green. Cells were exposed to blood +/−250 ppm CO for 15 min (a) representative flow cytometry dot plots and histograms; (b) Quantification as fold change versus control of n = 3 experiments. p < .0001 control versus blood, p < .0001 blood versus blood & CO. (c and d) Effect of HO-1 inhibition using SnPP IX (50 μM) on erythrophagocytosis in BV-2 microglia cells analyzed by flow cytometry after fluorescent blood labeling. Cells were exposed to blood +/−250 ppm CO for 30 min (c) representative flow cytometry dot plots and histograms; (d) quantification as fold change versus control of n = 3 experiments. p < .0001 blood versus SnPP & blood; p < .0001 blood versus blood & CO; p < .0001 blood & CO versus SnPP & blood & CO; p = n.s. SnPP & blood versus SnPP & blood & CO. (e) Effect of CO on erythrophagocytosis in *Hmox-1^fl/fl^*, *LyzMCre-Hmox1^fl/fl^* and *CD36^−/−^* microglia analyzed by flow cytometry after fluorescent blood labeling. Cells were exposed to blood +/−250 ppm CO for 15 min. (e) Quantification as fold change versus control of n = 3 experiments. p < .0001 blood *Hmox-1^fl/fl^* versus blood *LyzMCre-Hmox1^fl/fl^* and versus blood *CD36^−/−^*, p < .0001 blood & CO *Hmox-1^fl/fl^* versus blood & CO *LyzMCre-Hmox1^fl/fl^* and versus blood & CO *CD36^−/−^*, p < .0001 blood *Hmox-1^fl/fl^* versus blood & CO *Hmox-1^fl/fl^*
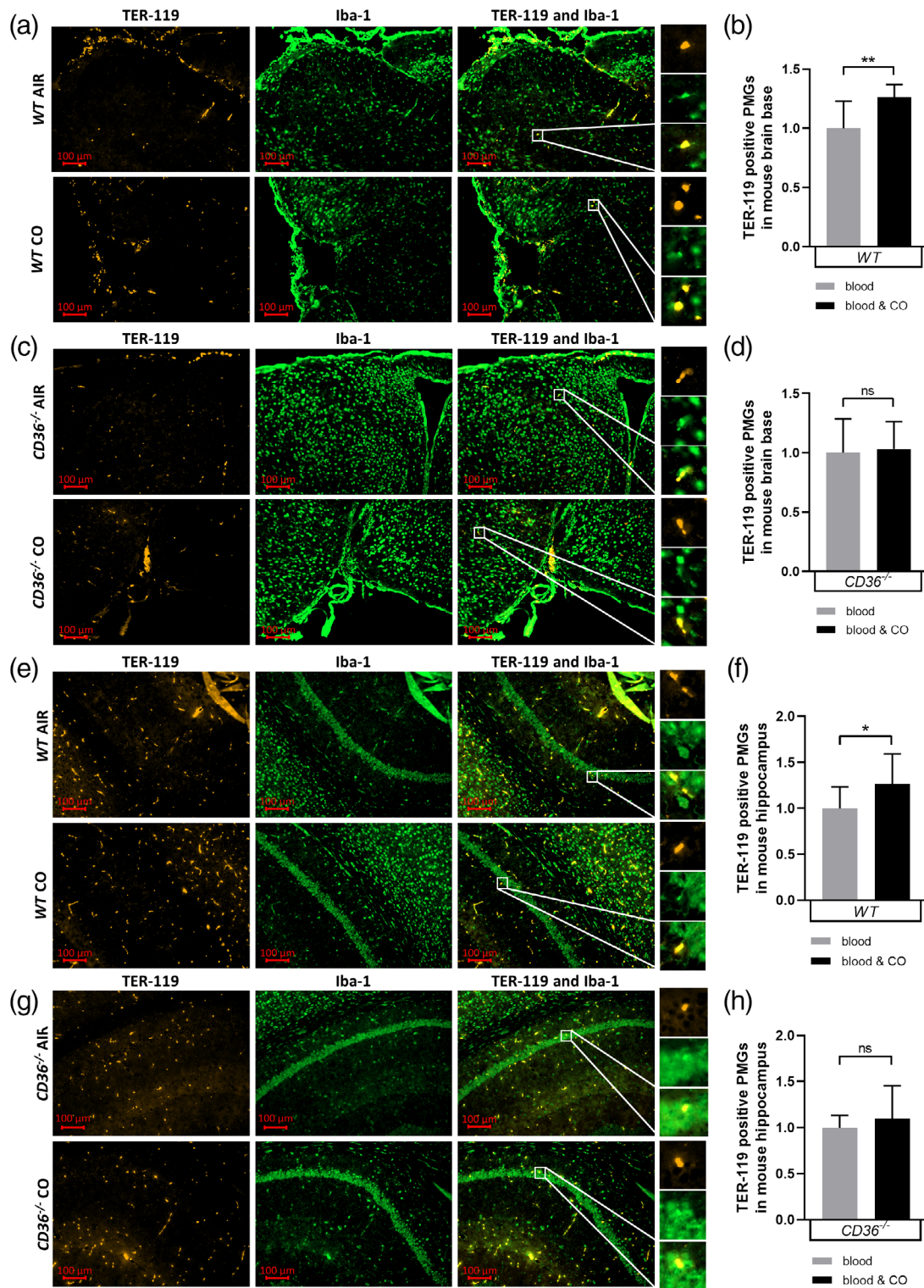
FIGURE 5 Colocalization of erythrocytes and microglia in brain regions of wild-type and CD36-deficient mice. (a–h) Colocalization of TER-119 positive erythrocytes and Iba-1 positive microglia in brain regions of *WT* and *CD36*$^{-/-}$ mice +/−CO (250 ppm 1 hr daily for 7 days post SAH induction). Representative coronal brain sections fluorescently stained for Iba-1 and TER-119 at the brain base (a and c) and in the hippocampus (e and g). Scale bars represent 100 μm. Quantification of colocalization of TER-119 and Iba-1 was done in immune fluorescence staining. Counting of TER-119 positive primary microglia in *WT* (b and f) and *CD36*$^{-/-}$ (d and h) mice +/−CO, normalized each to the blood control group without CO. $n = 3$ mice (4 pictures per mouse); $p = .0016$ brain base *WT* blood versus *WT* blood & CO; $p = .03$ hippocampus *WT* blood versus *WT* blood & CO. SAH, subarachnoid hemorrhage
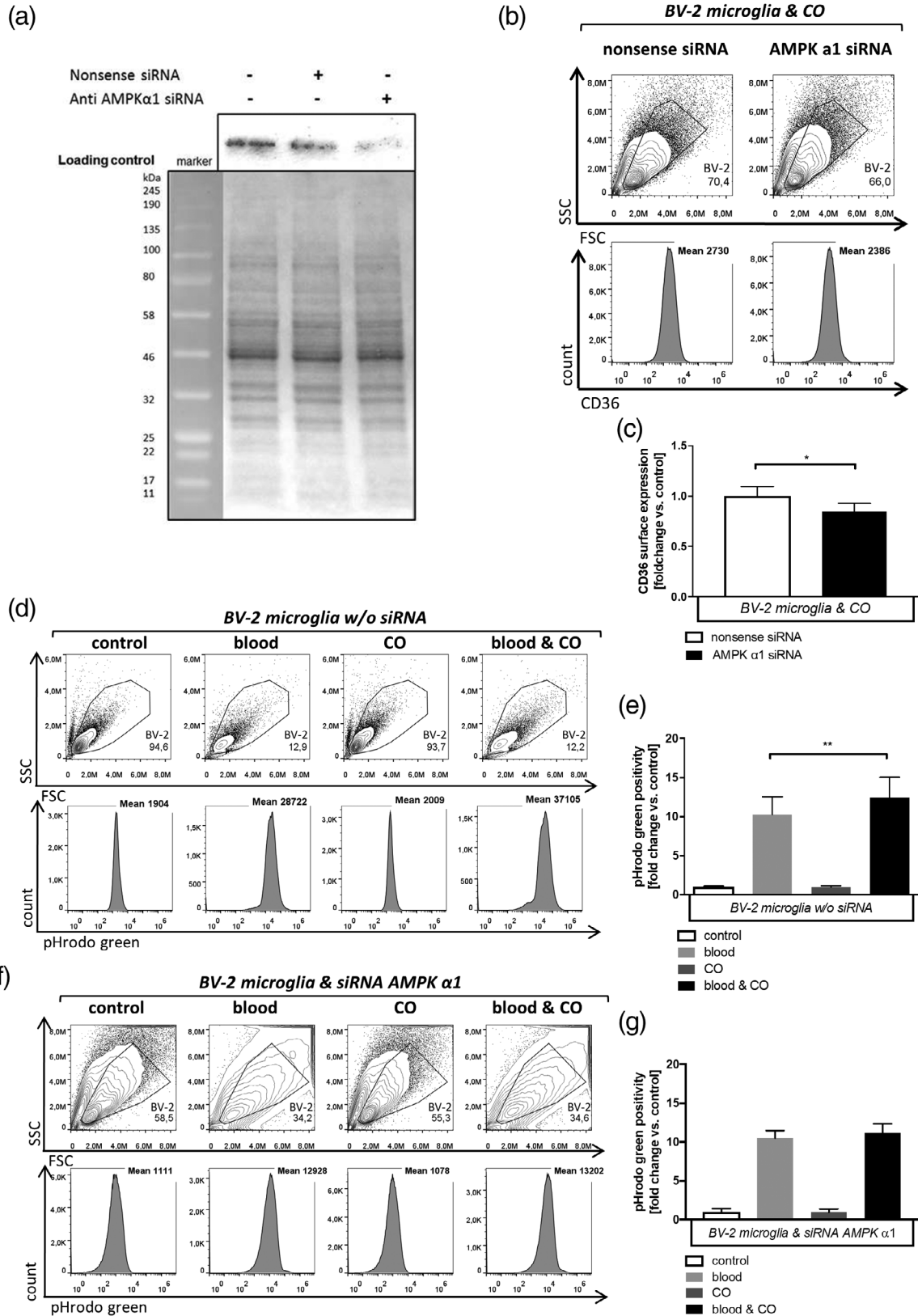
FIGURE 6 siRNA knockdown of AMPK abolishes the effects of CO on CD36 surface-expression and erythrophagocytosis. (a) Representative Western blot showing specific siRNA knockdown of catalytic AMPK subunit alpha-1. Lower panel shows blot loading control utilizing total protein staining. (b and c) CD36 surface expression measured by using flow cytometry (b, representative flow cytometry dot plots and histograms) and quantified as fold change versus control (c) in siRNA-treated BV-2 microglia cells +250 ppm CO, 5 min. n = 5 experiments per condition. p = .03 nonsense siRNA versus AMPK α1 siRNA. (d and e) Effect of CO on erythrophagocytosis in BV-2 microglia analyzed by flow cytometry after fluorescent blood labeling. Cells were exposed to blood +/−250 ppm CO for 1 hr (d: representative flow cytometry dot plots and histograms; (e) quantification as fold change versus control of n = 8 experiments). p = .003 blood versus blood & CO. (f and g) Abolished effect of CO on erythrophagocytosis in BV-2 microglia after specific siRNA (AMPK α1) treatment analyzed by flow cytometry. Cells were exposed to blood +/−250 ppm CO for 1 hr (f: representative flow cytometry dot plots and histograms; g: quantification as fold change vs. control of n = 8 experiments). p = .8 blood versus blood & CO
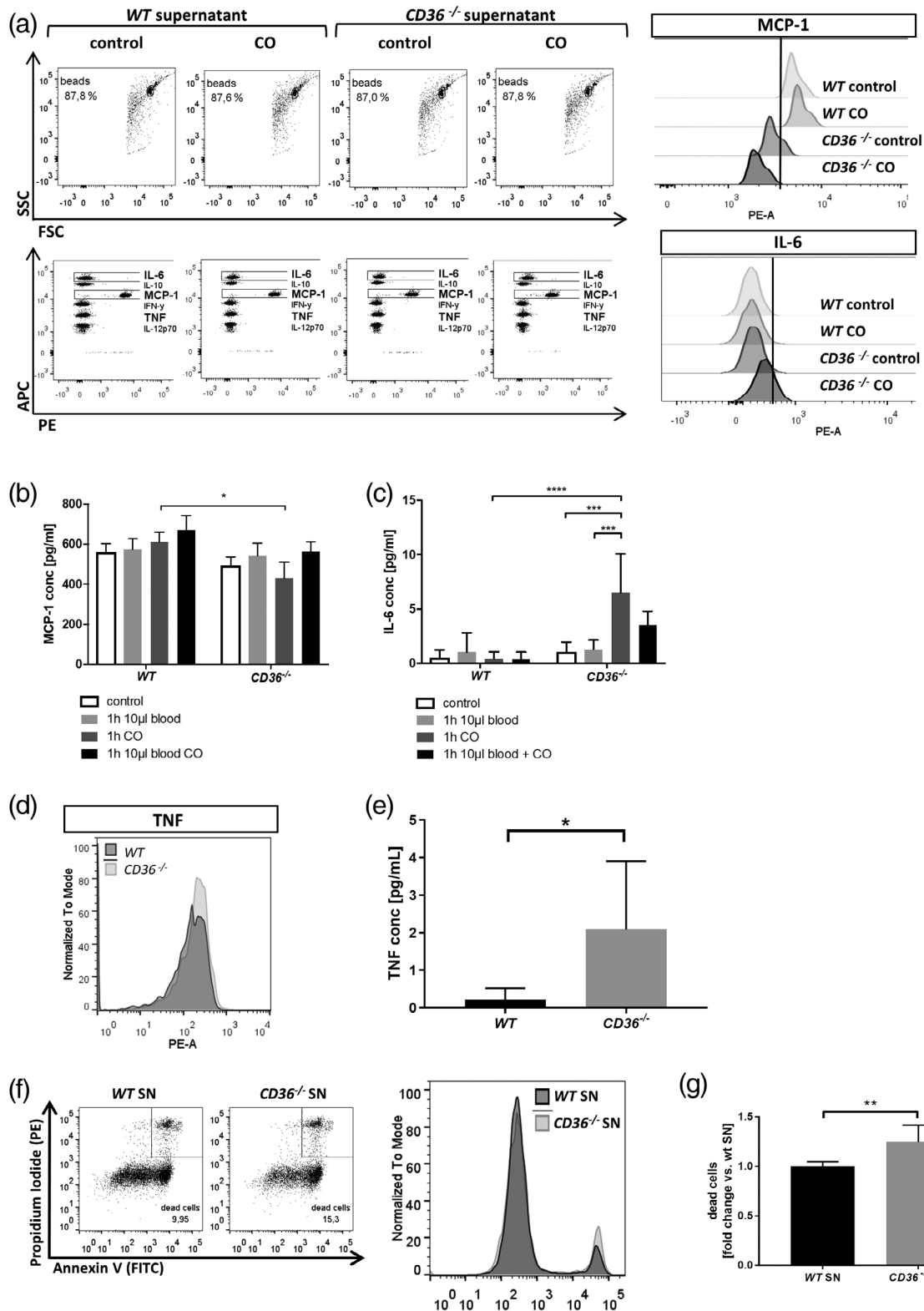
FIGURE 7 Secretion of inflammatory cytokines is altered in microglia deficient in CD36. (a) Representative flow cytometry plots analyzing the cytokine expression panel in *WT* versus *CD36*$^{-/-}$ microglia +/−CO 250 ppm, 1 hr. Histograms shown of MCP-1 and IL-6 *WT* versus *CD36*$^{-/-}$ microglia +/−CO 250 ppm, 1 hr. (b) Flow cytometry quantified as fold change versus control of microglial MCP-1 expression in *WT* versus *CD36*$^{-/-}$ microglia and CO 250 ppm, 1 hr. p = .04 for CO treatment *WT* versus CD36$^{-/-}$. (c) Flow cytometry quantified as fold change versus control of microglial IL-6 expression in *WT* and *CD36*$^{-/-}$ microglia +/−blood and CO 250 ppm, 1 hr. p < .0001 for CO treatment *WT* versus CD36$^{-/-}$; p = .0006 *CD36*$^{-/-}$ control versus CO; p = .001 *CD36*$^{-/-}$ blood versus CO. conc. = concentration (d) Representative flow cytometry plots analyzing the cytokine expression of TNF in *WT* versus *CD36*$^{-/-}$ microglia. (e) Flow cytometry quantified as fold change versus wild-type. Microglial TNF expression in *WT* and *CD36*$^{-/-}$ microglia. p = .03, n = 6. (f and g) Effect of factors released by microglia on neuronal cell death in neuronal HT22 cells in vitro analyzed by flow cytometry after Annexin V/Pi staining. HT22 cells were exposed to 10 µl blood and cultivated for 24 hr in 50% supernatant of cultured microglia isolated from either *WT* or *CD36*$^{-/-}$ mice. (f: Representative flow cytometry plots (SN = supernatant); g: quantification as fold change versus *WT* from total of n = 7 experiments; dead cells = Annexin and PI positive cells; p = .0028)
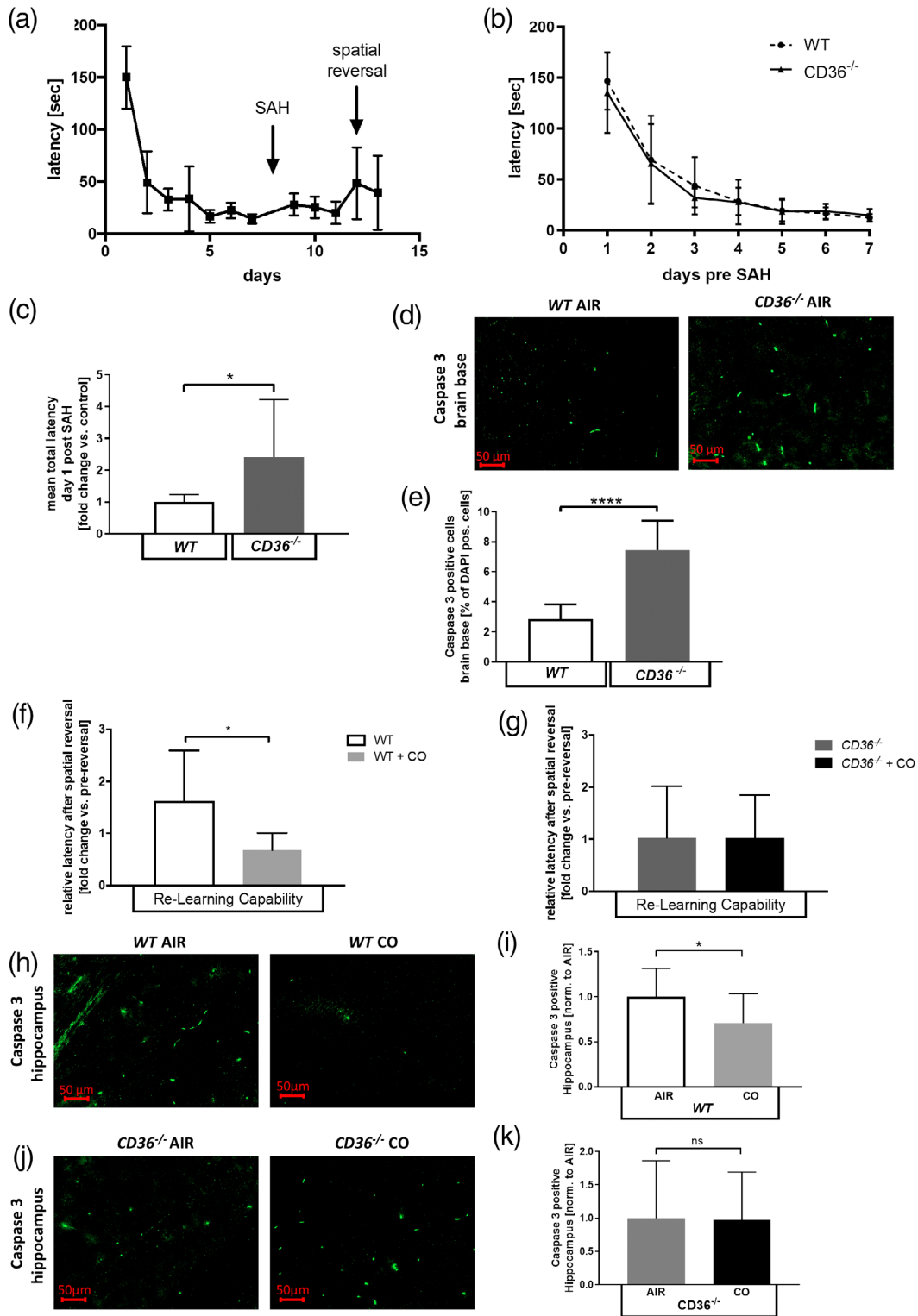
FIGURE 8 Legend on next page.

3.3 | Phosphorylated AMPK and CD36 surface expression increase with CO exposure

We next wanted to explore potential downstream targets for CO-induced ROS production. Activation of AMP-activated protein kinase (AMPK) has been suggested to be ROS-dependent (Jiang et al., 2013). We therefore analyzed the protein level of phosphorylated AMPK in BV-2 microglia as an indicator of activation by Western blot. CO exposure led to an increase in the amount of phosphorylated AMPK in microglia in vitro. When inhibiting ROS with NAC, CO could no longer increase phosphorylated AMPK (Figure 2a,b). The class B scavenger receptor CD36 is involved in hematoma resolution after hemorrhagic stroke (Fang et al., 2014; Flores et al., 2016; Mu et al., 2017). The exact mechanisms of how CD36 is regulated after hemorrhage are unclear. We hypothesized that surface expression of CD36 depends on the above described pathway involving HO-1, CO, and AMPK. When control microglia expressing HO-1 (*Hmox1$^{fl/fl}$*) were exposed to CO in vitro, an increase in CD36 surface expression was observed using flow cytometry (Figure 2c,d).

3.4 | Microglia deficient in HO-1 show impaired ROS production, less phosphorylated AMPK and CD36 surface expression in response to CO

To further test our hypothesis that microglial phagocytosis depends on the above described pathway involving CO, AMPK, and CD36, we next used a genetic approach. Microglia from mice with genetic HO-1-deficiency (*LyzMCre-Hmox1$^{fl/fl}$*) showed impaired production of ROS in response to CO compared to *Hmox1$^{fl/fl}$* microglia (Figure 3a,b). They displayed lower protein levels of phosphorylated AMPK at baseline (Figure 3c,d) and had reduced CD36 surface expression (Figure 3e,f). They did not respond to CO exposure with the upregulation of CD36 (Figure 3g,h), which was evident in control microglia expressing HO-1 (*Hmox1$^{fl/fl}$*).

3.5 | Microglia from HO-1-deficient mice are less capable of erythrophagocytosis compared to control microglia

To further explore whether these phenotypic changes are of functional relevance regarding the phagocytic capabilities, we labeled

erythrocytes with a fluorescent dye and measured phagocytosis by microglia. Phagocytosis was enhanced after exposing control microglia expressing HO-1 (*Hmox1$^{fl/fl}$*) to additional exogenous CO (Figure 4a,b). Pharmacological inhibition of HO using SnPP IX led to impaired microglial erythrophagocytosis that could not be compensated with exogenous CO (Figure 4c,d). SnPP IX administration inhibits both HO-1 and HO-2, leading to non-specific inhibition. We therefore used a genetic approach to specifically test the significance of HO-1 in erythrophagocytosis. Compared to control microglia with normal HO-1 expression (*Hmox1$^{fl/fl}$*) microglia with genetic HO-1-deficiency (*LyzMCre-Hmox1$^{fl/fl}$*) showed impaired erythrophagocytosis that could not be compensated with exogenous application of CO (Figure 4e).

3.6 | Microglial CD36-deficiency leads to impaired erythrophagocytosis that could not be rescued with exogenous CO

With evidence that CD36 surface-expression is influenced by the HO-1/CO enzyme system and that HO-1 in turn significantly influences erythrophagocytosis, we next studied the influence of CD36-deficiency on microglial phagocytic activity. Therefore, we isolated microglia from CD36 knockout mice and quantified phagocytosis after exposure to blood using FACS. Deficiency in CD36 resulted in profound impairment of erythrophagocytosis (Figure 4e) that could not be rescued with application of exogenous CO. To observe this effect in mice in vivo following hemorrhagic stroke, we analyzed colocalization of Iba-1 positive microglia and TER-119, which is expressed in erythrocytes, in a murine SAH model. Exogenous CO increased the number of microglia that colocalize with TER-119 in the brain base as well as the hippocampus in *WT* mice. In contrast, the colocalization of erythrocytes and microglia in *CD36$^{-/-}$* mice was not altered by exogenous CO (Figure 5a–h).

3.7 | Enhanced phagocytosis in microglial cells exposed to CO is abolished after genetically silencing AMPK

So far, our data suggest that microglial erythrophagocytosis depends on a ROS-dependent activation of AMPK leading to

FIGURE 8 Deterioration of spatial memory function and enhanced neuronal injury in CD36-deficient mice after experimental SAH. (a) Exemplary learning and performance curve in the barnes maze paradigm (here shown: *CD36$^{-/-}$* mice +CO). (b) Latency of *WT* and *CD36$^{-/-}$* mice in seconds (s) during the maze training time pre SAH. (c) Relative total latency times on day 1 after SAH in *WT* and *CD36$^{-/-}$* mice expressed as fold change versus *WT* controls. $n = 9$ animals per group; $p = .03$. (d) Representative coronal brain sections with cleaved Caspase 3 immunofluorescence staining of the brain base of *WT* and *CD36$^{-/-}$* mice. Scale bars represent 50 μm. (e) Quantification of the cleaved Caspase 3 immunofluorescence staining of the brain base 7 days after SAH in *WT* and *CD36$^{-/-}$* mice normalized to DAPI positive cells. $p = <.0001$. (f) Cognitive flexibility and re-learning capability measured after spatial reversal as relative latency times on day 13 compared to day 12 in *WT* animals +/−CO 250 ppm 1 hr treatment (daily). $n = 9$ animals per group, $p = .01$. (g) Cognitive flexibility and re-learning capability measured after spatial reversal as relative latency times on day 13 compared to day 12 in *CD36$^{-/-}$* animals +/−CO 250 ppm 1 hr treatment (daily). $n = 9$ animals per group, $p = .9$ *CD36$^{-/-}$* versus *CD36$^{-/-}$* + CO. (h–k) Cleaved Caspase 3 immunofluorescence staining of the hippocampus. (h and j) Representative coronal brain sections with cleaved Caspase 3 immunofluorescence staining of the hippocampus of *WT* (h) and *CD36$^{-/-}$* mice (j) +/−CO treatment (1 hr, 250 ppm daily). Scale bars represent 50 μm. (i and k) Quantification of the cleaved Caspase 3 immunofluorescence staining of the hippocampus 7 days after SAH in *WT* (i) and *CD36$^{-/-}$* mice (k) +/−CO treatment (1 hr, 250 ppm daily), $p = .045$ air *WT* versus CO *WT*. SAH, subarachnoid hemorrhage
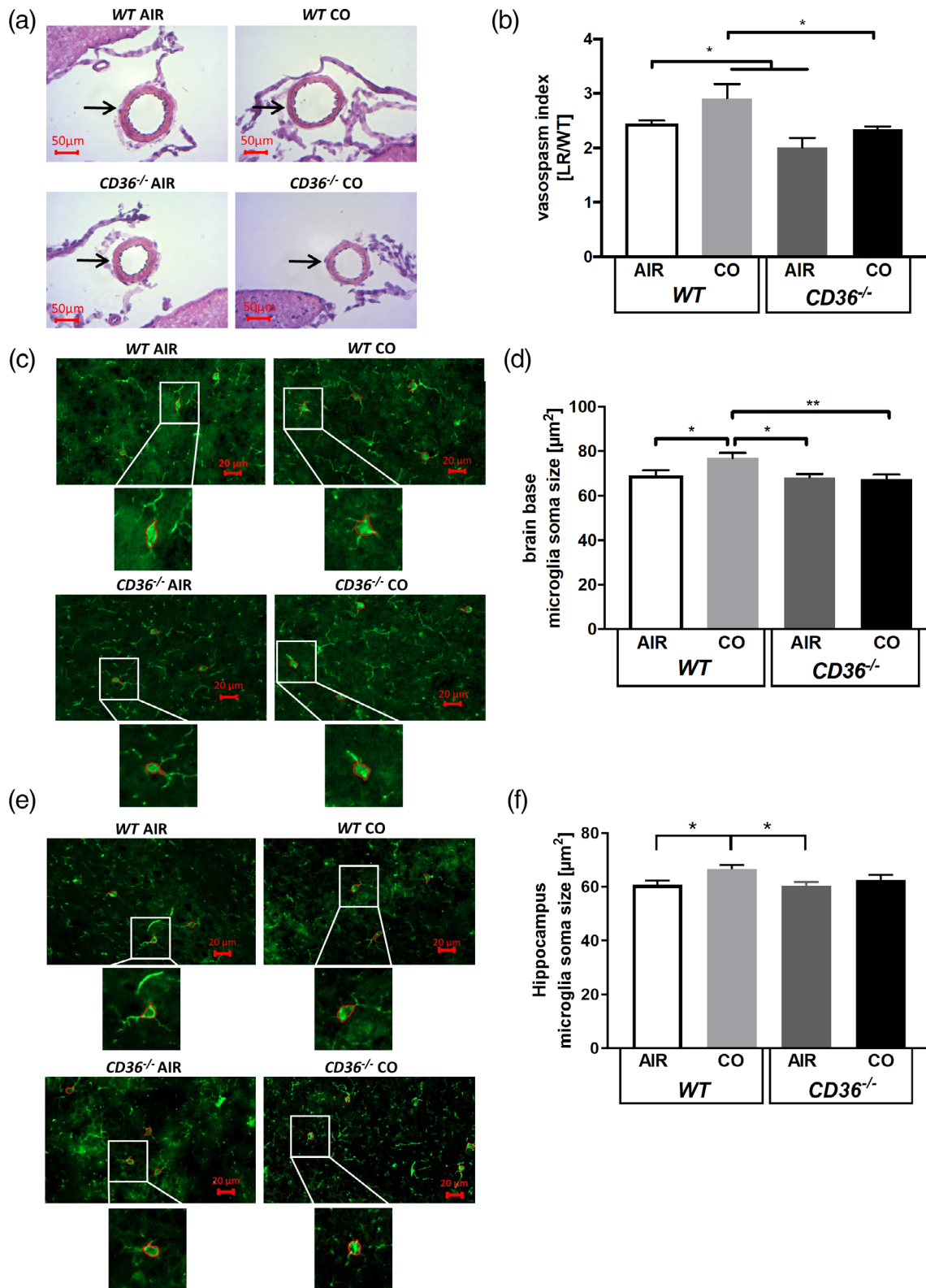
FIGURE 9 Legend on next page.

increased CD36 surface expression. To study that in fact AMPK bears a functional role, we used a transient genetic approach silencing the catalytic subunit alpha-1 in microglia. When the catalytic alpha-1 subunit of AMPK was specifically silenced (Figure 6a), microglia showed reduced CD-36 surface expression after CO exposure (Figure 6b,c). Cells transfected without siRNA showed an increase in phagocytosis in response to CO (Figure 6d,e) as observed previously. Microglia transfected with siRNA against AMPKα1 did not response to CO with increased erythrophagocytosis (Figure 6f,g).

3.8 | Secretion of inflammatory cytokines is altered in microglia deficient in CD36

Microglia as the immunocompetent cells of the brain derived from the myeloid lineage express cytokines that ultimately determine their function, including phagocytic activity. We hypothesized that functional differences observed between CD36-deficient and CD36-expressing microglia correlated with differences in their cytokine expression profiles. For this reason, we analyzed the cytokine expression profiles in both genotypes using a bead-based flow cytometry assay. Microglia deficient in CD36 differed in the expression of MCP-1 and IL-6 compared to wild-type microglia especially after exposure to CO (Figure 7a,c) with lower levels of MCP-1 and an increase in IL-6 expression. Additionally, CD36-deficient microglia showed higher TNF expression compares to wild-type (Figure 7d,e). We further analyzed the effect of this CD36 associated secretion of the pro-inflammatory factor TNF on neuronal cell survival. HT22 cells were exposed to blood and cultivated in supernatant of cultured microglia isolated from either *WT* or *CD36*$^{-/-}$ mice. Increased cell death was observed in neuronal cells cultivated with microglia supernatant of CD36-deficient mice compared to cultivation with wild-type microglia supernatant (Figure 7f,g). In summary, we showed that CD36 influences the secretion of inflammatory factors in microglia.

3.9 | Mice deficient in CD36 show enhanced neuronal apoptosis, altered inflammatory response in microglia and worsened functional outcome after experimental brain hemorrhage

With the pathway involving HO-1, CO, and CD36 established in vitro, we next investigated the role of CD36 and CO in a mouse model of hemorrhagic stroke in vivo. After 7 days of training on a maze, wild-type and CD36-deficient mice were subjected to subarachnoid hemorrhage with subsequent daily CO or air treatment. Spatial memory function was tested for 3 days post SAH induction. For testing cognitive flexibility, a reversal learning task was started 4 days post SAH on the maze (Figure 8a). CD36-deficient mice did show the same learning capacity as wild-type mice in the training process before SAH induction (Figure 8b). Indicating worsening of spatial memory recollection, *CD36*$^{-/-}$ mice showed higher latency times on the barnes maze tested 1 day after SAH (Figure 8c). As a histological correlate, this went along with increased neuronal apoptosis in *CD36*$^{-/-}$ animals at the site of blood deposition at the base of the brain analyzed by staining for cleaved Caspase-3 (Figure 8d, e). In the reversal learning task testing cognitive flexibility, we found that CO treatment improved relative latency times after spatial reversal in wild-type animals (Figure 8f). In contrast, CO treatment did not improve reversal learning in CD36-deficient mice (Figure 8g). In accordance with the observed re-learning capacity, neuronal apoptosis in the hippocampus was decreased by CO treatment in wild-type (Figure 8h,i) but not in CD36-deficient mice (Figure 8j,k). Furthermore, animals lacking CD36 showed exacerbated vasospasm compared to wild-type animals that could not be fully compensated by exogenous CO (Figure 9a,b). Additionally, CO treatment led to microglia activation observed by increased soma size at the brain base as well as the hippocampus in wild-type animals. On the contrary, CD36-deficient mice did not show altered microglia activation at the brain base or the hippocampus after CO treatment (Figure 9c–f).

FIGURE 9 Enhanced vasospasm in *CD36*$^{-/-}$ mice and elevated microglia activation in *WT* by exogenous CO after experimental SAH. (a) Representative H&E-stained cross-sections of the MCA at the base of the brain of *WT* and *CD36*$^{-/-}$ mice +/−CO treatment (1 hr, 250 ppm daily); arrows mark analyzed vessels; scale bars represent 50 μm. (b) Quantification of the vasospasm index (lumen radius/wall thickness) in the MCA 7 days after SAH in *WT* and *CD36*$^{-/-}$ mice +/−CO treatment (1 hr, 250 ppm daily). $n = 3$ mice per condition (three consecutive vessel cross sections per mouse), $p = .04$ air *WT* versus air *CD36*$^{-/-}$; $p = .03$ air *WT* versus CO *WT*; $p = .01$ CO *WT* versus CO *CD36*$^{-/-}$. (c) Representative coronal brain sections fluorescently stained for Iba-1 at the base of the brain of *WT* and *CD36*$^{-/-}$ mice +/−CO treatment (1 hr, 250 ppm daily), scale bars represent 20 μm. (d) Quantification of microglia-activation using morphological criteria described in the methods section (microglia soma size) at the base of the brain 7 days after SAH in *WT* and *CD36*$^{-/-}$ mice +/−CO treatment (1 hr, 250 ppm daily). $p = .04$ air *WT* versus CO *WT*; $p = .01$ CO *WT* versus air *CD36*$^{-/-}$; $p = .006$ CO *WT* versus CO *CD36*$^{-/-}$. (e) Representative coronal brain sections fluorescently stained for Iba-1 in the hippocampus of *WT* and *CD36*$^{-/-}$ mice +/−CO treatment (1 hr, 250 ppm daily). (f) Quantification of microglia-activation using morphological criteria described in the methods section (microglia soma size) in the hippocampus 7 days after SAH in *WT* and *CD36*$^{-/-}$ mice +/−CO treatment (1 hr, 250 ppm daily). Scale bars represent 20 μm; $p = .04$ air *WT* versus CO *WT*; $p = .03$ CO *WT* versus air *CD36*$^{-/-}$. MCA, middle-cerebral artery; SAH, subarachnoid hemorrhage

4 | DISCUSSION

The results from this study demonstrate that microglial erythrophagocytosis in response to brain hemorrhage is critically controlled by a HO-1 driven pathway that involves CO, mitochondrial ROS, AMP-activated kinase, and CD36. Genetic interference with several key components of the proposed pathway proofs the significance of the different components and how they interact. The central role of this pathway to relieve neuronal injury is highlighted by the fact that absence of CD36 leads to aggravated injury following hemorrhage in vivo. Emphasis should be placed on the fact that regarding timing and concentration of endogenous CO release via HO-1 induction, biological effects can be very different to those seen with exogenous CO: the pathway itself in vitro and neuronal outcome in vivo was modulated by exogenous CO, but deficiency in HO-1 could not be compensated by exogenous CO.

HO-1 induction represents a powerful stress response mechanism and its beneficial effects have been characterized in neuronal injury models (LeBlanc 3rd, Chen, Selim, & Hanafy, 2016; Saleem, Zhuang, Biswal, Christen, & Dore, 2008; Zhang et al., 2012). The mechanisms by which HO-1 influences neuroprotection, however, remain poorly understood and studies have mainly focused on its vasoactive (Ogawa et al., 2011) and anti-inflammatory (Foresti et al., 2013) properties. It is well known that the cell type in which HO-1 is mainly upregulated following ischemic or hemorrhagic injury, including SAH, are in fact microglia as the immunocompetent cells of the brain (P. Matz et al., 1996; Sutherland et al., 2009; Takeda et al., 1996; Turner et al., 1999). However, the function of microglial HO-1 following hemorrhagic stroke as not been thoroughly characterized. Here, we show that beside its catalytic role in heme degradation, HO-1 as the source of intracellular carbon monoxide serves as a signaling molecule to further enhance microglial uptake of erythrocytes via CD36. Of note, it has been shown before that HO-1 possesses distinct intracellular roles beyond its catalytic role in heme degradation as it might serve as a transcriptional regulator for genes controlling the response to oxidative stress (Collinson et al., 2011; Lin et al., 2007).

The HO-2 isoform is only expressed in neurons and endothelial cells and not upregulated following hemorrhage, further highlighting the specific role of microglial HO-1 in this context (Sutherland et al., 2009). This and the fact that endogenous HO-1-deficiency could not be compensated using exogenous CO gas emphasizes the notion that CO reaches specific intracellular and intracompartmental concentrations with critical time kinetics that cannot be compensated for by CO occurring from another source, that is, adjacent cells.

After defining the role of microglial HO-1 in erythrophagocytosis in previous work (Schallner et al., 2015) we were now able to elucidate an intracellular pathway that at least in part determines the regulation of erythrophagocytosis in microglia via HO-1. This pathway includes the production of mitochondrial ROS in response to CO production, the activation of ROS-responsive AMP-activated kinase, followed by regulation of CD36 surface expression. Most importantly, the significance of this pathway regarding neuronal outcome after hemorrhage is highlighted by our in vivo studies with absence of CD36 conferring a detrimental, CO-unresponsive genotype.

Mitochondrial ROS is produced in response to interference with intracellular oxidative phosphorylation and has been suggested as an inducer of neuronal damage (Cobb & Cole, 2015). However, its role as an intracellular signaling molecule cannot be understated (D'Autreaux & Toledano, 2007). ROS is known to induce activity of array pathways through redox-dependent modification (Schieber & Chandel, 2014). Interestingly, CO dose-dependently leads to increased ROS-production (Zuckerbraun et al., 2007), probably via its high affinity to heme-containing components of the respiratory chain. Our observation that CO exposure leads to a sudden, but transient burst in ROS production is in line with previous studies (Zuckerbraun et al., 2007). The transient nature of the effect can explain the fact that ROS-production was seen to a lesser extent after blood exposure alone even though we provide evidence that blood exposure leads to strong HO-1 induction and intracellular CO-production. This again points towards differences in intracompartmental distribution, actual concentration and time kinetics in exogenous versus endogenous CO.

AMP-activated Kinase (AMPK) is an enzyme critically involved in cellular metabolism and homeostasis (Herzig & Shaw, 2018). It is regulated by changes in the cellular redox-state and hence its activity is responsive to changes in ROS-production (Jiang et al., 2013). We were able to show that AMPK responds to CO-exposure with changes in the protein level of its phosphorylated state and activity. AMPK has been studied in chemotaxis of macrophages (Park et al., 2013), but here we define a new role by linking AMPK activity to CD36 surface expression and erythrophagocytosis in microglia.

Microglial expression of the scavenger receptor CD36 has been linked to microglial phagocytosis in intracerebral hemorrhage (Fang et al., 2014; Zhao et al., 2007) and other brain pathologies (Li et al., 2015; Yamanaka et al., 2012) before. Its expression increases in hemorrhage and deficiency has been associated with increased neuronal injury (Fang et al., 2014). However, regulation of CD36 surface expression on microglia has not been linked to HO-1/CO signaling before and here we provide a novel explanation for the CD36-mediated effects in brain hemorrhage.

SAH is a subtype of hemorrhagic stroke that accounts for only 10% of all strokes. But due to its still high mortality and early onset of age, it accounts for more than one third of all stroke-related lost life years (Rincon et al., 2013). Many patients suffer from long term cognitive deficits that are due to delayed cerebral ischemia. It has been a longstanding doctrine that DCI happens secondarily to cerebral vasospasm, usually seen 7 days after SAH. However, this view has been challenged recently by the fact that the effective treatment of cerebral vasospasm cannot improve cognitive deficit and DCI (Macdonald et al., 2008). This points towards a different pathophysiology in SAH, putting emphasize on neuroinflammation as one of the factors critically contributing to neuronal injury.

The role of the neuroinflammatory response executed by microglia in neuronal injury is controversial, as increased inflammation can be detrimental by induction of neuronal apoptosis (Hanafy, 2013), but can also be neuroprotective (Vinet et al., 2012).

The fate neuronal cells will take in response to inflammation most likely depends on the type of injury and also on the exact mode of microglial activation and polarization, which is in analogy to peripheral macrophages. Here we provide evidence that CD36 can also serve as a downstream-signaling receptor that determines the array of inflammatory cytokines produced by microglia, as the setup of cytokines produced was different in wild-type and CD36-deficient microglia. More specifically, we found genotype-specific differences in the expression of MCP-1 and IL-6 after CO exposure as well as TNF, which hints towards a more pro-inflammatory polarization in CD36-deficient microglia, as MCP-1 causes microglial migration and proliferation without a direct activation of the pro-inflammatory response (Hinojosa, Garcia-Bueno, Leza, & Madrigal, 2011; Yang et al., 2011). This could lead to a different polarization of microglia which effects phagocytosis as well as neuronal survival. This is in accordance with the pathological phenotype observed in CD36-deficient mice.

In vivo, $CD36^{-/-}$ mice showed aggravated injury that was not responsive to CO. CD36 expression has been associated with neuronal injury previously (Fang et al., 2014) but has not been linked to the HO-1/CO axis or phagocytic function of microglia. In contrast, CO in wild-type conditions executed significant neuroprotection. This is in line with the previous work of our own group and others (Biermann, Lagreze, Dimitriu, Stoykow, & Goebel, 2010; Schallner et al., 2015; Zeynalov & Dore, 2009). These potent neuroprotective effects of CO and the HO-1 signaling axis warrant further clinical studies investigating potential use in humans. In the future, inhaled CO might contribute to treating this deleterious hemorrhagic brain injury.

CONFLICT OF INTEREST

The authors declare no potential conflict of interest.

DATA AVAILABILITY STATEMENT

The data that support the findings of this study are available from the corresponding author upon reasonable request.

ORCID

Sandra Kaiser https://orcid.org/0000-0003-1667-1311
Nils Schallner https://orcid.org/0000-0003-2120-788X

REFERENCES

Almeida, A. S., Queiroga, C. S., Sousa, M. F., Alves, P. M., & Vieira, H. L. (2012). Carbon monoxide modulates apoptosis by reinforcing oxidative metabolism in astrocytes: ROLE OF Bcl-2. *The Journal of Biological Chemistry*, *287*(14), 10761–10770. https://doi.org/10.1074/jbc.M111.306738

Biermann, J., Lagreze, W. A., Dimitriu, C., Stoykow, C., & Goebel, U. (2010). Preconditioning with inhalative carbon monoxide protects rat retinal ganglion cells from ischemia/reperfusion injury. *Investigative Ophthalmology & Visual Science*, *51*(7), 3784–3791. https://doi.org/10.1167/iovs.09-4894

Chen, G., Fang, Q., Zhang, J., Zhou, D., & Wang, Z. (2011). Role of the Nrf2-ARE pathway in early brain injury after experimental subarachnoid hemorrhage. *Journal of Neuroscience Research*, *89*(4), 515–523. https://doi.org/10.1002/jnr.22577

Clark, J. E., Foresti, R., Sarathchandra, P., Kaur, H., Green, C. J., & Motterlini, R. (2000). Heme oxygenase-1-derived bilirubin ameliorates postischemic myocardial dysfunction. *American Journal of Physiology. Heart and Circulatory Physiology*, *278*(2), H643–H651.

Cobb, C. A., & Cole, M. P. (2015). Oxidative and nitrative stress in neurodegeneration. *Neurobiology of Disease*, *84*, 4–21. https://doi.org/10.1016/j.nbd.2015.04.020

Collinson, E. J., Wimmer-Kleikamp, S., Gerega, S. K., Yang, Y. H., Parish, C. R., Dawes, I. W., & Stocker, R. (2011). The yeast homolog of heme oxygenase-1 affords cellular antioxidant protection via the transcriptional regulation of known antioxidant genes. *The Journal of Biological Chemistry*, *286*(3), 2205–2214. https://doi.org/10.1074/jbc.M110.187062

D'Autreaux, B., & Toledano, M. B. (2007). ROS as signalling molecules: Mechanisms that generate specificity in ROS homeostasis. *Nature Reviews. Molecular Cell Biology*, *8*(10), 813–824. https://doi.org/10.1038/nrm2256

Fadok, V. A., Warner, M. L., Bratton, D. L., & Henson, P. M. (1998). CD36 is required for phagocytosis of apoptotic cells by human macrophages that use either a phosphatidylserine receptor or the vitronectin receptor (alpha v beta 3). *Journal of Immunology*, *161*(11), 6250–6257.

Fang, H., Chen, J., Lin, S., Wang, P., Wang, Y., Xiong, X., & Yang, Q. (2014). CD36-mediated hematoma absorption following intracerebral hemorrhage: Negative regulation by TLR4 signaling. *Journal of Immunology*, *192*(12), 5984–5992. https://doi.org/10.4049/jimmunol.1400054

Flores, J. J., Klebe, D., Rolland, W. B., Lekic, T., Krafft, P. R., & Zhang, J. H. (2016). PPARgamma-induced upregulation of CD36 enhances hematoma resolution and attenuates long-term neurological deficits after germinal matrix hemorrhage in neonatal rats. *Neurobiology of Disease*, *87*, 124–133. https://doi.org/10.1016/j.nbd.2015.12.015

Foresti, R., Bains, S. K., Pitchumony, T. S., de Castro Bras, L. E., Drago, F., Dubois-Rande, J. L., ... Motterlini, R. (2013). Small molecule activators of the Nrf2-HO-1 antioxidant axis modulate heme metabolism and inflammation in BV2 microglia cells. *Pharmacological Research*, *76*, 132–148. https://doi.org/10.1016/j.phrs.2013.07.010

Fukuda, K., Panter, S. S., Sharp, F. R., & Noble, L. J. (1995). Induction of heme oxygenase-1 (HO-1) after traumatic brain injury in the rat. *Neuroscience Letters*, *199*(2), 127–130.

Goebel, U., Siepe, M., Mecklenburg, A., Stein, P., Roesslein, M., Schwer, C. I., ... Loop, T. (2008). Carbon monoxide inhalation reduces pulmonary inflammatory response during cardiopulmonary bypass in pigs. *Anesthesiology*, *108*(6), 1025–1036. https://doi.org/10.1097/ALN.0b013e3181733115

Hanafy, K. A. (2013). The role of microglia and the TLR4 pathway in neuronal apoptosis and vasospasm after subarachnoid hemorrhage. *Journal of Neuroinflammation*, *10*, 83. https://doi.org/10.1186/1742-2094-10-83

Herzig, S., & Shaw, R. J. (2018). AMPK: Guardian of metabolism and mitochondrial homeostasis. *Nature Reviews. Molecular Cell Biology*, *19*(2), 121–135. https://doi.org/10.1038/nrm.2017.95

Hijdra, A., Van Gijn, J., Stefanko, S., Van Dongen, K. J., Vermeulen, M., & Van Crevel, H. (1986). Delayed cerebral ischemia after aneurysmal subarachnoid hemorrhage: Clinicoanatomic correlations. *Neurology*, *36*(3), 329–333.

Hinojosa, A. E., Garcia-Bueno, B., Leza, J. C., & Madrigal, J. L. (2011). CCL2/MCP-1 modulation of microglial activation and proliferation. *Journal of Neuroinflammation*, *8*, 77. https://doi.org/10.1186/1742-2094-8-77

Jiang, S., Park, D. W., Stigler, W. S., Creighton, J., Ravi, S., Darley-Usmar, V., & Zmijewski, J. W. (2013). Mitochondria and AMP-activated

protein kinase-dependent mechanism of efferocytosis. *The Journal of Biological Chemistry*, *288*(36), 26013–26026. https://doi.org/10.1074/jbc.M113.489468

King, J. T., Jr. (1997). Epidemiology of aneurysmal subarachnoid hemorrhage. *Neuroimaging Clinics of North America*, *7*(4), 659–668.

Kuroki, M., Kanamaru, K., Suzuki, H., Waga, S., & Semba, R. (1998). Effect of vasospasm on heme oxygenases in a rat model of subarachnoid hemorrhage. *Stroke*, *29*(3), 683–688 discussion 688-689.

LeBlanc, R. H., 3rd, Chen, R., Selim, M. H., & Hanafy, K. A. (2016). Heme oxygenase-1-mediated neuroprotection in subarachnoid hemorrhage via intracerebroventricular deferoxamine. *Journal of Neuroinflammation*, *13*(1), 244. https://doi.org/10.1186/s12974-016-0709-1

Li, X., Melief, E., Postupna, N., Montine, K. S., Keene, C. D., & Montine, T. J. (2015). Prostaglandin E2 receptor subtype 2 regulation of scavenger receptor CD36 modulates microglial Abeta42 phagocytosis. *The American Journal of Pathology*, *185*(1), 230–239. https://doi.org/10.1016/j.ajpath.2014.09.016

Lin, Q., Weis, S., Yang, G., Weng, Y. H., Helston, R., Rish, K., ... Dennery, P. A. (2007). Heme oxygenase-1 protein localizes to the nucleus and activates transcription factors important in oxidative stress. *The Journal of Biological Chemistry*, *282*(28), 20621–20633. https://doi.org/10.1074/jbc.M607954200

Macdonald, R. L., Higashida, R. T., Keller, E., Mayer, S. A., Molyneux, A., Raabe, A., ... Kassell, N. (2011). Clazosentan, an endothelin receptor antagonist, in patients with aneurysmal subarachnoid haemorrhage undergoing surgical clipping: A randomised, double-blind, placebo-controlled phase 3 trial (CONSCIOUS-2). *Lancet Neurology*, *10*(7), 618–625. https://doi.org/10.1016/S1474-4422(11)70108-9

Macdonald, R. L., Kassell, N. F., Mayer, S., Ruefenacht, D., Schmiedek, P., Weidauer, S., ... Pasqualin, A. (2008). Clazosentan to overcome neurological ischemia and infarction occurring after subarachnoid hemorrhage (CONSCIOUS-1): Randomized, double-blind, placebo-controlled phase 2 dose-finding trial. *Stroke*, *39*(11), 3015–3021. https://doi.org/10.1161/STROKEAHA.108.519942

Matz, P., Turner, C., Weinstein, P. R., Massa, S. M., Panter, S. S., & Sharp, F. R. (1996). Heme-oxygenase-1 induction in glia throughout rat brain following experimental subarachnoid hemorrhage. *Brain Research*, *713*(1-2), 211–222.

Matz, P. G., Weinstein, P. R., & Sharp, F. R. (1997). Heme oxygenase-1 and heat shock protein 70 induction in glia and neurons throughout rat brain after experimental intracerebral hemorrhage. *Neurosurgery*, *40*(1), 152–160 discussion 160-152.

McGilvray, I. D., Serghides, L., Kapus, A., Rotstein, O. D., & Kain, K. C. (2000). Nonopsonic monocyte/macrophage phagocytosis of Plasmodium falciparum-parasitized erythrocytes: A role for CD36 in malarial clearance. *Blood*, *96*(9), 3231–3240.

Motterlini, R., & Otterbein, L. E. (2010). The therapeutic potential of carbon monoxide. *Nature Reviews. Drug Discovery*, *9*(9), 728–743. https://doi.org/10.1038/nrd3228

Mu, Q., Wang, L., Hang, H., Liu, C., & Wu, G. (2017). Rosiglitazone pre-treatment influences thrombin-induced phagocytosis by rat microglia via activating PPARgamma and CD36. *Neuroscience Letters*, *651*, 159–164. https://doi.org/10.1016/j.neulet.2017.04.038

Ogawa, T., Hanggi, D., Wu, Y., Michiue, H., Tomizawa, K., Ono, S., ... Steiger, H. J. (2011). Protein therapy using heme-oxygenase-1 fused to a polyarginine transduction domain attenuates cerebral vasospasm after experimental subarachnoid hemorrhage. *Journal of Cerebral Blood Flow and Metabolism*, *31*(11), 2231–2242. https://doi.org/10.1038/jcbfm.2011.87

Otterbein, L. E., Kolls, J. K., Mantell, L. L., Cook, J. L., Alam, J., & Choi, A. M. (1999). Exogenous administration of heme oxygenase-1 by gene transfer provides protection against hyperoxia-induced lung injury. *The Journal of Clinical Investigation*, *103*(7), 1047–1054. https://doi.org/10.1172/JCI5342

Otterbein, L. E., Mantell, L. L., & Choi, A. M. (1999). Carbon monoxide provides protection against hyperoxic lung injury. *The American Journal of Physiology*, *276*(4 Pt 1), L688–L694.

Park, D. W., Jiang, S., Tadie, J. M., Stigler, W. S., Gao, Y., Deshane, J., ... Zmijewski, J. W. (2013). Activation of AMPK enhances neutrophil chemotaxis and bacterial killing. *Molecular Medicine*, *19*, 387–398. https://doi.org/10.2119/molmed.2013.00065

Rincon, F., Rossenwasser, R. H., & Dumont, A. (2013). The epidemiology of admissions of nontraumatic subarachnoid hemorrhage in the United States. *Neurosurgery*, *73*(2), 217–222; discussion 212-213. https://doi.org/10.1227/01.neu.0000430290.93304.33

Saleem, S., Zhuang, H., Biswal, S., Christen, Y., & Dore, S. (2008). *Ginkgo biloba* extract neuroprotective action is dependent on heme oxygenase 1 in ischemic reperfusion brain injury. *Stroke*, *39*(12), 3389–3396. https://doi.org/10.1161/STROKEAHA.108.523480

Schallner, N., Fuchs, M., Schwer, C. I., Loop, T., Buerkle, H., Lagreze, W. A., ... Goebel, U. (2012). Postconditioning with inhaled carbon monoxide counteracts apoptosis and neuroinflammation in the ischemic rat retina. *PLoS One*, *7*(9), e46479. https://doi.org/10.1371/journal.pone.0046479

Schallner, N., Pandit, R., LeBlanc, R., 3rd, Thomas, A. J., Ogilvy, C. S., Zuckerbraun, B. S., ... Hanafy, K. A. (2015). Microglia regulate blood clearance in subarachnoid hemorrhage by heme oxygenase-1. *The Journal of Clinical Investigation*, *125*(7), 2609–2625. https://doi.org/10.1172/JCI78443

Schieber, M., & Chandel, N. S. (2014). ROS function in redox signaling and oxidative stress. *Current Biology*, *24*(10), R453–R462. https://doi.org/10.1016/j.cub.2014.03.034

Shimada, Y., Tsunoda, H., Zang, L., Hirano, M., Oka, T., & Tanaka, T. (2009). Synergistic induction of heme oxygenase-1 by nicaraven after subarachnoid hemorrhage to prevent delayed cerebral vasospasm. *European Journal of Pharmacology*, *620*(1-3), 16–20. https://doi.org/10.1016/j.ejphar.2009.08.009

Song, R., Kubo, M., Morse, D., Zhou, Z., Zhang, X., Dauber, J. H., ... Choi, A. M. (2003). Carbon monoxide induces cytoprotection in rat orthotopic lung transplantation via anti-inflammatory and anti-apoptotic effects. *The American Journal of Pathology*, *163*(1), 231–242. https://doi.org/10.1016/S0002-9440(10)63646-2

Sutherland, B. A., Rahman, R. M., Clarkson, A. N., Shaw, O. M., Nair, S. M., & Appleton, I. (2009). Cerebral heme oxygenase 1 and 2 spatial distribution is modulated following injury from hypoxia-ischemia and middle cerebral artery occlusion in rats. *Neuroscience Research*, *65*(4), 326–334. https://doi.org/10.1016/j.neures.2009.08.007

Suwatcharangkoon, S., Meyers, E., Falo, C., Schmidt, J. M., Agarwal, S., Claassen, J., & Mayer, S. A. (2016). Loss of consciousness at onset of subarachnoid hemorrhage as an important marker of early brain injury. *JAMA Neurology*, *73*(1), 28–35. https://doi.org/10.1001/jamaneurol.2015.3188

Takeda, A., Kimpara, T., Onodera, H., Itoyama, Y., Shibahara, S., & Kogure, K. (1996). Regional difference in induction of heme oxygenase-1 protein following rat transient forebrain ischemia. *Neuroscience Letters*, *205*(3), 169–172.

Tayem, Y., Green, C. J., Motterlini, R., & Foresti, R. (2014). Isothiocyanate-cysteine conjugates protect renal tissue against cisplatin-induced apoptosis via induction of heme oxygenase-1. *Pharmacological Research*, *81*, 1–9. https://doi.org/10.1016/j.phrs.2014.01.001

Turner, C. P., Panter, S. S., & Sharp, F. R. (1999). Anti-oxidants prevent focal rat brain injury as assessed by induction of heat shock proteins (HSP70, HO-1/HSP32, HSP47) following subarachnoid injections of lysed blood. *Brain Research. Molecular Brain Research*, *65*(1), 87–102.

van Lieshout, J. H., Dibue-Adjei, M., Cornelius, J. F., Slotty, P. J., Schneider, T., Restin, T., ... Kamp, M. A. (2017). An introduction to the pathophysiology of aneurysmal subarachnoid hemorrhage.

Neurosurgical Review, 41, 917–930. https://doi.org/10.1007/s10143-017-0827-y

Vieira, H. L., Queiroga, C. S., & Alves, P. M. (2008). Pre-conditioning induced by carbon monoxide provides neuronal protection against apoptosis. *Journal of Neurochemistry, 107*(2), 375–384. https://doi.org/10.1111/j.1471-4159.2008.05610.x

Vinet, J., Weering, H. R., Heinrich, A., Kalin, R. E., Wegner, A., Brouwer, N., ... Biber, K. (2012). Neuroprotective function for ramified microglia in hippocampal excitotoxicity. *Journal of Neuroinflammation, 9,* 27. https://doi.org/10.1186/1742-2094-9-27

Wang, H. Q., Xu, Y. X., & Zhu, C. Q. (2012). Upregulation of heme oxygenase-1 by acteoside through ERK and PI3 K/Akt pathway confer neuroprotection against beta-amyloid-induced neurotoxicity. *Neurotoxicity Research, 21*(4), 368–378. https://doi.org/10.1007/s12640-011-9292-5

Yabluchanskiy, A., Sawle, P., Homer-Vanniasinkam, S., Green, C. J., Foresti, R., & Motterlini, R. (2012). CORM-3, a carbon monoxide-releasing molecule, alters the inflammatory response and reduces brain damage in a rat model of hemorrhagic stroke. *Critical Care Medicine, 40*(2), 544–552. https://doi.org/10.1097/CCM.0b013e31822f0d64

Yamanaka, M., Ishikawa, T., Griep, A., Axt, D., Kummer, M. P., & Heneka, M. T. (2012). PPARgamma/RXRalpha-induced and CD36-mediated microglial amyloid-beta phagocytosis results in cognitive improvement in amyloid precursor protein/presenilin 1 mice. *The Journal of Neuroscience, 32*(48), 17321–17331. https://doi.org/10.1523/JNEUROSCI.1569-12.2012

Yang, G., Meng, Y., Li, W., Yong, Y., Fan, Z., Ding, H., ... Ke, Z. J. (2011). Neuronal MCP-1 mediates microglia recruitment and neurodegeneration induced by the mild impairment of oxidative metabolism. *Brain Pathology, 21*(3), 279–297. https://doi.org/10.1111/j.1750-3639.2010.00445.x

Zeynalov, E., & Dore, S. (2009). Low doses of carbon monoxide protect against experimental focal brain ischemia. *Neurotoxicity Research, 15*(2), 133–137. https://doi.org/10.1007/s12640-009-9014-4

Zhang, F., Wang, S., Zhang, M., Weng, Z., Li, P., Gan, Y., ... Chen, J. (2012). Pharmacological induction of heme oxygenase-1 by a triterpenoid protects neurons against ischemic injury. *Stroke, 43*(5), 1390–1397. https://doi.org/10.1161/STROKEAHA.111.647420

Zhao, X., Sun, G., Zhang, J., Strong, R., Song, W., Gonzales, N., ... Aronowski, J. (2007). Hematoma resolution as a target for intracerebral hemorrhage treatment: Role for peroxisome proliferator-activated receptor gamma in microglia/macrophages. *Annals of Neurology, 61*(4), 352–362. https://doi.org/10.1002/ana.21097

Zuckerbraun, B. S., Billiar, T. R., Otterbein, S. L., Kim, P. K., Liu, F., Choi, A. M., ... Otterbein, L. E. (2003). Carbon monoxide protects against liver failure through nitric oxide-induced heme oxygenase 1. *The Journal of Experimental Medicine, 198*(11), 1707–1716. https://doi.org/10.1084/jem.20031003

Zuckerbraun, B. S., Chin, B. Y., Bilban, M., d'Avila, J. C., Rao, J., Billiar, T. R., & Otterbein, L. E. (2007). Carbon monoxide signals via inhibition of cytochrome c oxidase and generation of mitochondrial reactive oxygen species. *The FASEB Journal, 21*(4), 1099–1106. https://doi.org/10.1096/fj.06-6644com